Miniaturization and embedding of soliton-based electro-optically addressable photonic arrays

A. D'Ercole, E. Palange,[a),b)] E. DelRe,[c)] A. Ciattoni, B. Crosignani,[c)] and A. J. Agranat[d)]
Dipartimento di Fisica, Universita' dell'Aquila, 67010 L'Aquila, Italy and Istituto Nazionale Fisica della Materia, Unita' dell'Aquila, 67010 L'Aquila, Italy

(Received 26 April 2004; accepted 19 July 2004)

We achieved the soliton-based miniaturized integration of electro-optic devices in a photorefractive paraelectric bulk crystal, by driving self-trapping through an external bias field in a top-sided electrode geometry. The ensuing spatially resolved electric field manifests a localized voltage-dependent region in which a quasi-uniform field leads to screening-like self-trapped waves at considerably low voltages without sample miniaturization, along with their electro-optic beam manipulation. By replicating the electrode structure, our achievements constitute the basic building block that paves the way to digitally addressable volume photonic manipulator arrays. © *2004 American Institute of Physics*. [DOI: 10.1063/1.1795359]

Photorefractive spatial solitons[1] have been recently implemented to achieve electro-optically activated beam manipulation functions, such as intensity modulation and two-channel routing, the devices themselves self-integrated in the bulk.[2,3] The basic idea is to first generate a soliton in an otherwise homogeneous crystal, and then to use the refractive index pattern to guide longer wavelength, nonphotorefractively active, beams, for which it is effectively permanent.[4] At this stage, a quadratic electro-optic response allows the activation and alteration of the original pattern, by changing the external bias, a process which provides device functionality during readout.[5] This is the result of the beating between the traces of the soliton-supporting space-charge field and the now controlling external bias.

The optical circuitry is at once integrated in the bulk crystal volume, transparent at infrared wavelengths, and compatible with a fast response. Previous results have reproduced the basic electro-optic functions presently achieved through integrated $LiNbO_3$ technology. Solitons, in turn, hold the key to a qualitatively different technology, in which *guided* beam handling and processing occurs in a fully three-dimensional *bulk* environment.[6] The intrinsic localization and robustness of the soliton beams should allow the exploitation of the entire crystal volume to achieve elaborate and massively dense optical routing structures, with particular advantages for future generations of miniaturized transparent devices.

Where recent endeavors point in this direction,[7,8] no physical mechanism has been devised to allow for the possibility of imprinting a *given* steering pattern in the volume, formed through different localized soliton processes, and to subsequently address and *electro-optically* activate them through appropriate low switching voltages. The weakness of henceforth investigated soliton and soliton-array manifestations lies in the fact that these emerge through the screening of a constant homogeneous external bias field, delivered through two opposite electrodes deposited on the opposite lateral faces of the sample. This leads to a field orthogonal to the beam propagation axis, in common to all solitons, not allowing for any form of spatially resolved control on the nonlinear process that does not involve (slow) charge redistribution.[8,9]

Moreover, the exact balancing of diffraction and self-lensing, for a given micron-sized soliton or multisoliton structure, implies an external electric field, which both drives photorefractive charge migration and determines the spatially resolved electro-optic response, of the order of several kV/cm (Ref. 10) (see Ref. 11 for a review) that translates into characteristic values of applied voltage of the order of a kV.

Microfabrication of a dedicated guiding geometry, as generally done for $LiNbO_3$, limits the advantages peculiar to solitary waves in bulk. Furthermore, in ferroelectric crystals, altering the standard geometry can activate depolarization, a process leading to domain enucleation which does not evidently affect a paraelectric crystal.

We demonstrate a viable avenue based on delivering the bias voltage through a single facet geometry, with all the electrodes deposited side-by-side, during the nonlinear propagation writing stage and in the subsequent routing stage. Electrostatically, in this configuration, the values of external bias required to achieved kV/cm fields can be considerably reduced by microscopically reducing the electrode distance. Furthermore, by tailoring the electrode geometry, we can achieve a quasiarbitrary spatial pattern of the bias electric field, up to several hundred microns inside the sample.

Physically, this attractive condition implies a considerably altered optical self-action, in view of the fact that the photorefractive charges, which mediated the self-induced index pattern, are set to respond and drift in a now elaborate and *spatially resolved external electric field*, and that the system is inherently vectorial: response, now not constrained by geometry, can be made to exhibit qualitatively different features, which *a priori* need not include solitons. In turn, our present aim is focused on finding the conditions for screening-like soliton formation, and associated nonlinear

[a)]Electronic mail: palange@ing.univaq.it
[b)]Dipartimento di Ingegneria Elettrica, Universita' dell'Aquila, 67040 Monteluco di Roio (L'Aquila), Italy.
[c)]Istituto Nazionale Fisica della Materia, Unita' di Roma "La Sapienza," 00185 Rome, Italy.
[d)]Department of Applied Physics, Hebrew University of Jerusalem, Jerusalem 91904, Israel.

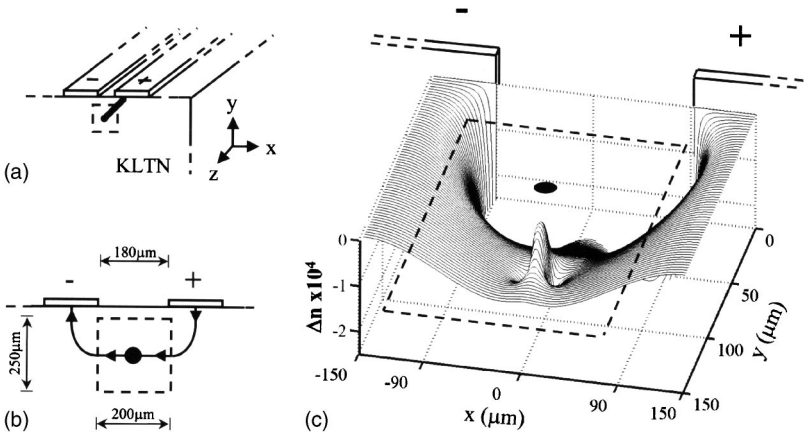

FIG. 1. Top-sided electrode geometry: schematic (a); detail of soliton-activated region (b); and numerical prediction of trapping pattern $\Delta n(x,y)$ (c).

and electro-optic phenomenology. We implement the geometry illustrated in Fig. 1(a), which constitutes, in our scheme, the basic building block to the more complex and elaborate addressable photonic array. Since there is no possibility of analytically fixing the boundary conditions, we rely on a numerical approach to predict the now intrinsically vectorial space charge field **E** induced by the light beam. We consider the standard photorefractive model[11]

$$\nabla \cdot \left[-(I + I_b) \nabla \varphi + (K_B T/q) \nabla I \right] = 0, \tag{1}$$

where φ is the space charge electrostatic potential ($\mathbf{E} = -\nabla \varphi$), I the light intensity distribution, I_b the background illumination intensity, K_B the Boltzmann constant, T the temperature, q the electron charge and $\nabla = \partial_x \hat{\mathbf{e}}_x + \partial_y \hat{\mathbf{e}}_y$. We self-consistently restrict investigation to z-invariant intensity distributions I that characterize solitons, reducing Eq. (1) to a the two-dimensional transverse xy plane. Self-action is the result of the electro-optic index-pattern modulation $\Delta n = -(1/2) n^3 g \epsilon_0^2 (\epsilon_r - 1)^2 (\partial \varphi / \partial x)^2$, where n is the zero-field refractive index, $g = g_{xxxx}$ is the dominant component of the quadratic electro-optic tensor g_{ijkl} for an x-polarized launch beam, ϵ_0 is the vacuum dielectric constant, and ϵ_r is the relative sample low-frequency dielectric constant.[12]

We specialize predictions to our experiments, which hinge on a $3^{(x)} \times 2.4^{(y)} \times 1^{(z)}$ mm sized sample of Cu and V co-doped potassium–lithium–niobate–tantalate (KLTN) crystal, at a temperature $T = 16\ ^\circ\mathrm{C}$, 4° above the ferroparaelectric transition, where $n \simeq 2.4$, $g \simeq 0.12\ \mathrm{m}^4\ \mathrm{C}^{-2}$, and $\epsilon_r \simeq 1.5 \times 10^4$.[12] The top-sided electrodes were tailored on the $3^{(x)} \times 1^{(z)}$ mm facet, with an intraelectrode 180 μm gap [see Fig. 1(b)]. The beam was a continuous-wave argon ion 50 mW x-polarized laser, operating at $\lambda = 514$ nm whose intensity distribution is approximated by a Gaussian of intensity full width at half-maximum (FWHM) $\Delta x = \Delta y = 7$ μm and intensity ratio $I_{\max}/I_b = 5$.

Numerical results indicate that a region emerges in which the generally inhomogeneous bias field is quasiuniform. Although it is sufficiently extended to encompass the diffracting beam, its position (and size) is dependent on the applied voltage. Therefore, in contrast to standard geometries, soliton formation involves the matching of two (as opposed to one) electrostatic conditions: that the quasiuniform region, associated with the given values of external bias, be in proximity with the soliton launch position, and that its value coincide with that required to self-trap.

For example, an external bias of $V_{\mathrm{sol}} = 80$ V will lead to a needle trapping index pattern $\Delta n(x,y)$, locally resembling the standard one,[13] if the propagating beam is launched 110 μm from the crystal edge, as plotted in Fig. 1(c). In general, calculations identify a relationship between the vertical launch position and the soliton supporting V_{sol}, that, for launches up to several hundred microns into the bulk, are more than one order of magnitude lower than those required in the standard configurations. For example, 50 μm from the edge, the predicted $V_{\mathrm{sol}} \simeq 40$ V.

Experimental results for a launch ~ 50 μm from the top edge, are reported in Fig. 2. For a zero applied voltage, the beam diffracts to 15 μm after the 1 mm propagation along the z axis, corresponding to approximately two diffraction lengths [see Fig. 2(b)]. As predicted, two-dimensional self-trapping is achieved for a $V_{\mathrm{sol}} \simeq 40-50$ V, after a buildup time of approximately $\tau_s \simeq 120$ s, for a 1 μW launch.

Similar self-trapping phenomenology was observed from 50 to 300 μm from the top edge, with voltages ranging from 40 to 160 V, leading to a screening-like soliton supporting region inside the crystal of $200^{(x)} \times 250^{(y)}$ μm^2, schematically illustrated in Figs. 1(b) and 1(c). The measured values of V_{sol} at different distances from the edge are shown in Fig. 2(d). Beams launched less than 50 μm from the top edge experienced distortive edge effects, whereas trapping

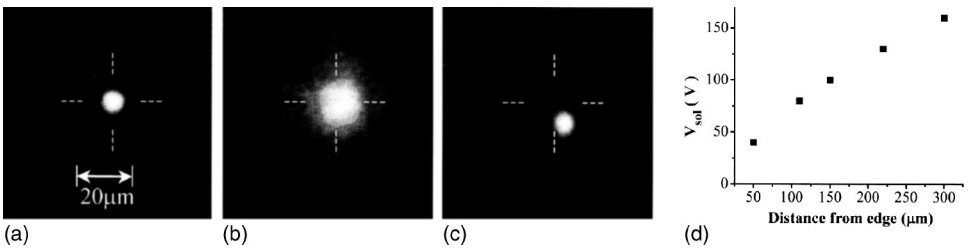

FIG. 2. Soliton formation: intensity distribution of the input 7 μm FWHM beam (a); diffraction at output face (b); and self-trapped soliton for $V_{\mathrm{sol}} = 40$ V (c). Note the soliton slippage in the vertical direction due to the slight index gradient [see Fig. 1(c)], combined to the standard self-bending process. Measured V_{sol} vs the distance from the crystal edge is plotted in (d).

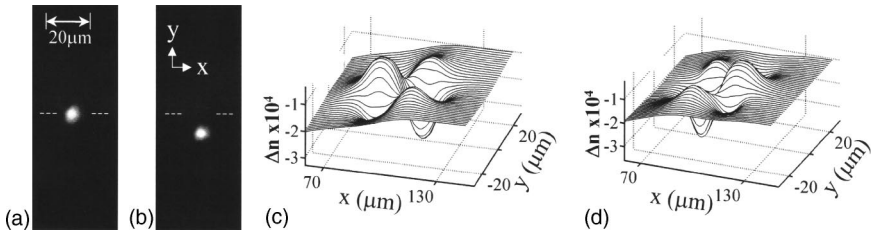

FIG. 3. Embedded routing: output intensity distribution for $V_{act}=80$ V (a); for $V_{act}=-80$ V (b); (c), (d) the respective calculated index patterns $\Delta n(x,y)$.

beyond the 300 μm limit required values of applied voltage leading to the dielectric breakdown of the air. In the horizontal dimension, the region is determined by the emergence of *y*-oriented components, which considerably weaken self-action. By impinging on the pattern with a less intense 50 *n*W readout beam, which activates charge displacement only for times greater than 20 τ_s, we are able to achieve electro-optic25 dB attenuation. This occurs because the soliton pattern, activated for $V_{act}=V_{sol}$, reverts to a defocusing structure for $V_{act}=0$.[2,5]

The next step was to implement our results to miniaturize electro-optic beam manipulation and switching, realizing a two-mode router using two solitons of opposite electro-optic response,[2,3] achieved within the same soliton-active region. The writing stage is accomplished in two steps: in the first, a single soliton is formed 90 μm from the crystal edge, with an appropriate value of V_{sol}; subsequently, a second soliton is formed with an opposite biasing voltage $-V_{sol}$ at 110 μm from the edge, such that they are vertically stacked. The first soliton is now activated and guides for a $V_{act}=V_{sol}$, the second being antiguiding, whereas for $V_{act}=-V_{sol}$, the roles are inverted, attaining the required routing, when the read beam is launched between the two, at 100 μm from the edge. We congruently modify the model of Eq. (1), allowing the prediction of the space-charge field induced both by the soliton and a previously attained charge distribution. Switching results and the relative predicted electro-optic patterns are shown in Fig. 3.

We now pass to the issue of the extendability, both in the horizontal (surface) and in the vertical (volume) directions. A first variant, which contains the ingredients that allow a progressive sophistication of circuitry towards elaborate elements, such as embedded Mach–Zehnder-type structures, is shown in Fig. 4. In this case, we generated three vertically stacked solitons, the top [Fig. 4(a)] and bottom [Fig. 4(b)] of positive electro-optic response, whereas the central one is negative [Fig. 4(c)]. The structure is achieved through an appropriate sequence which allows the formation of the 7 $\times 20$ μm^2 system, and forms an electroactivated beamsplitter for $V_{act}=V_{sol}$ [Fig. 4(e)], or, alternatively a waveguide for $V_{act}=-V_{sol}$ [Fig. 4(f)], when the read beam is launched on the central soliton. Horizontal scalability can be achieved replicating each device with a further electrode stage, as shown in Fig. 4(d). Preliminary results for three electrodes confirm that independent solitons form, generating two separately addressable devices. Linear and nonlinear interaction among beams in different soliton-activated regions has not yet been addressed, since we are in the process of developing the required micron-level-tailored electrodes.

In conclusion, our investigation demonstrates that top-sided electrodes can allow spatial photorefractive soliton formation for quasidigital voltages in an extended crystal volume. They further support different geometries with a varied spectrum of electro-optical manipulative functions. The intrinsic miniaturization which derives from the spatially resolved bias conditions, opens the way to addressable arrays of photonic devices. In fact, we have demonstrated both vertically stacked, Fig. 3, and horizontally distributed soliton circuitry, embedded in the bulk volume.

Research was funded by the Italian Istituto Nazionale Fisica della Materia (INFM) through the "Solitons Embedded in Holograms" (SEH) Project, and by the Italian Ministry of Research through the "Space-Time Effects" Basic Research FIRB project. A.D. and E.P. acknowledge the support of the DEWS Center for Excellence (L'Aquila).

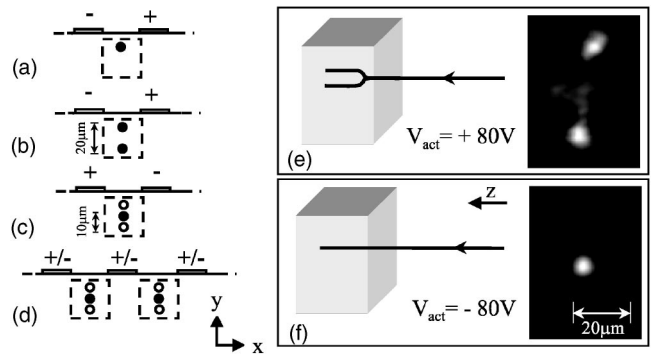

FIG. 4. Waveguide/beamsplitter function: schematic of writing stages (a)–(c); horizontal replication (d); schematic of guiding pattern and output intensity distribution of light for $V_{act}=80$ V, for which the splitter is electroactivated (e); and for $V_{act}=-80$ V, for which the central waveguide is electroactivated (f).

[1] M. Segev, B. Crosignani, A. Yariv, and B. Fischer, Phys. Rev. Lett. **68**, 923 (1992).
[2] E. DelRe, B. Crosignani, P. Di Porto, E. Palange, and A. J. Agranat, Opt. Lett. **27**, 2188 (2002).
[3] E. DelRe, E. Palange, and A. J. Agranat, J. Appl. Phys. **95**, 3822 (2004).
[4] M. F. Shih, M. Segev, and G. Salamo, Opt. Lett. **21**, 931 (1996).
[5] E. DelRe, M. Tamburrini, and A. J. Agranat, Opt. Lett. **25**, 963 (2000).
[6] G. I. Stegeman and M. Segev, Science **286**, 1518 (1999).
[7] J. W. Fleischer, M. Segev, N. K. Efremidis, and D. N. Christodoulides, Nature (London) **422**, 147 (2003).
[8] J. Petter, J. Schroder, D. Trager, and C. Denz, Opt. Lett. **28**, 438 (2003).
[9] P. Dittrich, G. Montemezzani, P. Bernasconi, and P. Gunter, Opt. Lett. **24**, 1508 (1999).
[10] M. Segev, G. C. Valley, B. Crosignani, P. DiPorto, and A. Yariv, Phys. Rev. Lett. **73**, 3211 (1994).
[11] *Spatial Solitons*, edited by S. Trillo and W. Torruellas (Springer, Berlin, 2001), Chap. 4.
[12] E. DelRe, M. Tamburrini, M. Segev, E. Refaeli, and A. J. Agranat, Appl. Phys. Lett. **73**, 16 (1998).
[13] S. Gatz and J. Herrmann, Opt. Lett. **23**, 1176 (1998).